2024 IEEE International Conference on Robotics and Automation (ICRA 2024)
May 13-17, 2024. Yokohama, Japan

Development of Variable Transmission Series Elastic Actuator for Hip Exoskeletons

Tianci Wang, Hao Wen, Zaixin Song, Zhiping Dong, and Chunhua Liu, *Senior Member, IEEE*

***Abstract*— Series Elastic Actuator-based exoskeleton can offer precise torque control and transparency when interacting with human wearers. Accurate control of SEA-produced torques ensures the wearer's voluntary motion and supports the implementation of multiple assistive paradigms. In this paper, a novel variable transmission series elastic actuator (VTSEA) is developed to meet torque-speed requirements in different exoskeleton-assisted locomotion modes, such as running, walking, sit-to-stand, and stand-to-sit. The VTSEA features a SEA-coupled variable transmission ratio adjusting mechanism and works between three discrete levels of transmission ratio depending on the user's initiative. The proposed prototype can also improve transparency in human-robot interaction. Also, an accurate torque controller with inertial compensation is developed for the VTSEA via the singular perturbation theory, and its stability is proved. The feasibility of the proposed VTSEA prototype and the precise output torque performance of VTSEA are verified by experiments.**

I. Introduction

Stable and accurate torque delivery, high modularity, low mechanical resistance, and high transparency are significant needs for the actuators of assistive devices, including low-extremity exoskeletons [1]. For the sake of the need for flexible interaction and effective torque control, series elastic actuators (SEAs) for wearable robotics have recently attracted much attention because of their uniqueness compared with conventional actuators, including stable torque measurement, low mechanical impedance, and effective disturbance rejection [2, 3]. Since the primary duty of a lower-limb exoskeleton is to transmit the torque and speed to the user [4], precise torque and speed delivery is a significant consideration in lower-limb exoskeleton development for patients with locomotion disorders. Daniel's research shows the importance of accurate auxiliary speed and torque for the wearer because they affect the execution efficiency of the user's daily living activities and the metabolic cost of the user's walking [5].

This work was supported in part by a grant by a grant (Project No. JCYJ20210324134005015) from the Science Technology and Innovation Committee of Shenzhen Municipality, Shenzhen, China; in part by a Collaborative Research Fund (CRF Project No. C1052-21GF) from the Research Grants Council, Hong Kong SAR; and in part by RGC Research Fellow Scheme (RGC Ref. No.: RFS2223-1S05) from Research Grants Council, Hong Kong SAR. (*Corresponding author: Chunhua Liu).

T. Wang, H. Wen, Z. Dong, and C. Liu are with Shenzhen Research Institute, City University of Hong Kong, Shenzhen, 5180507, China. Also, they are with the School of Energy and Environment, City University of Hong Kong, Hong Kong SAR, China. (e-mail: Tianci.Wang@my.cityu.edu.hk; hao.wen@my.cityu.edu.hk; zhiping.dong@my.cityu.edu.hk; corresponding author, C. Liu: +852-34422885; fax: +852-34420688; e-mail: chunliu@cityu.edu.hk).

Z. Song is with State Key Laboratory of Ultra-precision Machining Technology, Department of Industrial and Systems Engineering, The Hong Kong Polytechnic University, Hong Kong SAR. (e-mail: zaixin.song@polyu.edu.hk).

Except for assistive torque and speed, the wearable robot should output assistive force only when assistance is required and generate zero force when not needed, which is usually called transparency in physical human-robot interaction [6]. Transparency is considered a key factor in the development of assistive robotics [7]. At present, to provide transparency effectively, assistive robots adopt various control algorithms, such as impedance/admittance control [8, 9], time delay control [10], and interaction force feedback control [11, 12]. However, those algorithms have stability issues due to the inherent parameters drifting, model uncertainty, or measuring noise, and they often cause unreliable transparency. Moreover, the human-exoskeleton system is time-varying nonlinear and is susceptible to complicated human motion [13]. Finally, actuators developed for wearable robotics should exhibit high repeatability, robustness, shock tolerance, and safety [14]. Considering the above reasons, we developed a variable transmission series elastic actuator to disengage the mechanical connection between the actuator and the user under the user's control. The unique property of our proposed actuator is that transparency is achieved via a variable transmission ratio mechanical design rather than a control algorithm. Other studies try to achieve transparency by introducing additional electrical components such as commercial clutch [15-17], but it will increase control system complexity compared with our proposed variable transmission series elastic actuator (VTSEA), which allows for control of assistance torque, speed, and transparency with low control complexity, high stability and repeatability.

For an accurate torque delivery of SEA, multiple strategies have been developed for SEA control, such as singular perturbation control [18], Markovian transparency control [19], adaptive oscillator control [20], radial-basis neural network sliding mode control [21], cascade PI control [7, 22], and disturbance observer control [23, 24]. Because the torsion spring serves as a transducer between the spring deformation and torque in the SEA, the spring can accurately control the assistive torque by employing traditional position controllers. For those assistive robotics driven by SEAs, the merit of the singular perturbation theory (SPT) is particularly fascinating [2, 17, 25]. This is because the SEA exhibits two response timescales: fast actuator dynamics (i.e., elastic force) and slow actuator dynamics (i.e., link position). The core idea is to separate time scales of the system dynamics, yielding a quasi-steady-state model for tracking control and a boundary-layer for resonance suppression [26]. The SPT can be brought into controller design for two subsystems dissociable by regarding the fast actuator dynamics as a perturbation of the slow actuator dynamics [25]. The robustness of the SPT-based controller is guaranteed only if the torsion stiffness of the spring is large enough [27, 28]. At present, most SEAs developed for wearable robotics have a

spring stiffness of approximately 400 N.m/rad [29-31]. For increasing compliance in the human-exoskeleton interaction, the developed VTSEA in this article has a stiffness lower than 60 Nm/rad, which makes the SPT-based controller design very challenging. By introducing a transmission ratio shifting mechanism, a new torque control problem is introduced when the transmission ratio switches because of the low stiffness of the torsion spring. Moreover, the low stiffness VTSEA may also cause mechanical vibration and bring a security risk to the user. Moreover, the SPT-based controller is susceptible to the model parameters drifting [32]. Since the load side is directly connected with the human user which influences the model dynamics, it is not easy to directly utilize the existing SPT-based controller on hip exoskeletons. To outstretch the SPT approach to our proposed VTSEA with low spring stiffness and inevitable switching disturbance, in this paper, we propose an SPT-based controller with inertial compensation. This controller can modulate the VTSEA's dynamic response using inertial compensation.

Based on the previous studies, this paper presents an accurate SPT-based controller with inertial compensation for a VTSEA-driven exoskeleton. The merits for the human user with the VTSEA-driven exoskeleton are to allow for mechanical transparency and multiple torque-speed output. The accuracy, stability, shock tolerance, and repeatability of the exoskeleton are ensured by both mechanical design and controller implementation.

II. Materials and Methods

A. Hardware Platform

This part gives an introduction to the hip exoskeleton named HopeExo, and the VTSEA design employed in this exoskeleton. Fig. 1 describes the mechanical design of the hip exoskeleton and VTSEA. Hip flexion/extension of the exoskeleton is realized by two actuators, each for one-side hip flexion-extension, fixed on the lateral leg.

The wearable robotic is convenient to don, doff, and attach to the user at three primary positions: leg, pelvis, and torso. Thigh supports are employed to loosely restrict the upper leg and provide standing. The exoskeleton suspender support is fixed to the user's upper body using a pelvis and shoulder straps. Two cuffs per leg at the thigh attach the exoskeleton to the leg. To accommodate different wearers, the exoskeleton contains a series of adjustable mechanisms, including retractable structures in the thigh, waist, and back, and a sliding rail mechanism at the pelvis.

TABLE I. MAIN CHARACTERISTICS OF THE HIP EXOSKELETON

Features	Values	Unit
Range of Motion	-60~60	degree
Maximum Continuous Torque	133.2	N.m.
Peak velocity	12	rotation/sec
Output Torque Resolution	0.0028	Nm
Joint mass	5.98	Kg
Transmission Ratio	1:6, 1:36,0	/

B. VTSEA Module

Multiple motors can be used to drive the actuator [33-37]. The proposed VTSEA is actuated by a brushless DC motor via a two-stage planetary gear, as shown in Fig. 1 (c). The motor is a high-power-density rotating flat brushless motor (T-motor) with a power of 1300 W and a continuous torque of 3.7 N.m. The maximum transmission ratio can be reached 36:1, leading to an output torque of up to 133.2 N.m, output rotational speed of 4320 deg/s, and peak torques of up to 396 Nm for durations on the order of a few seconds. The well-custom-made torque spring connects the secondary carrier with the joint output end. The torsional spring is specially developed to meet the target stiffness requirements while minimizing weight. The series of elastic-driven joints have two angular encoders, which are used for the motor side and load side displacement measurement. Three current sensors are employed to measure the motor current. Two IMUs are used to measure the joint acceleration.

To our ends, there were two main causes for integrating a transmission ratio adjustment mechanism into the SEA. First, the added mechanism is able to improve mechanical transparency, guaranteeing that the wearable device outputs assistive force only when assistance is required and generates zero force when not needed. Second, as shown in Fig. 2, the VTSEA can be switched to a low, zero, or high transmission ratio to meet the torque-speed needs of different activities of daily life, including sit-to-stand, stand-to-sit, walking, running, etc.

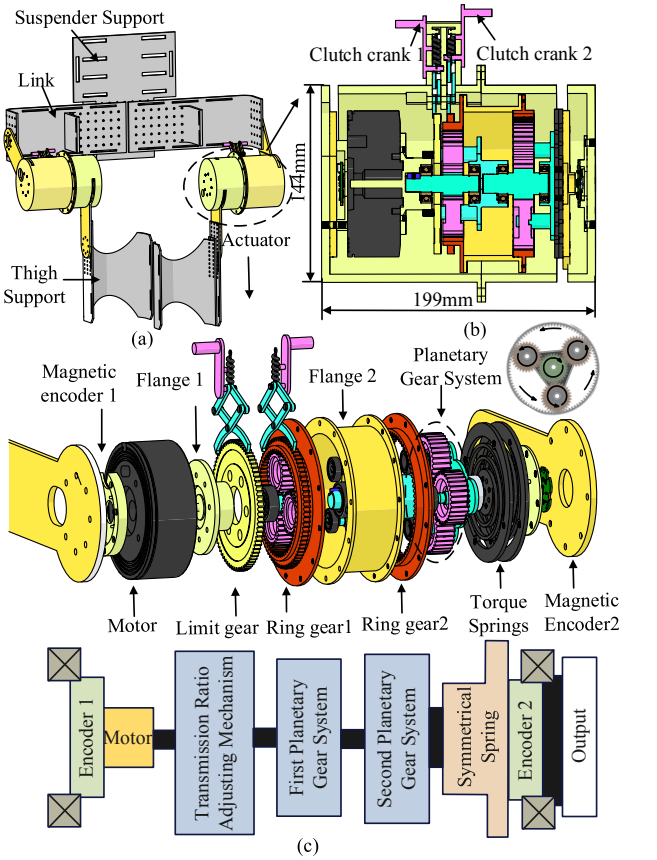

Fig. 1. Overview of the HopeExo. (a) Hip Exoskeleton CAD model. (b) Section view of VTSEA. (c) Main modules of VTSEA.

C. SPT-based Torque Controller Design for VTSEA

Fig. 3 presents the dynamic model of the VTSEA system. The dynamics of an n-degree-of-freedom SEA-driven assistive robot are described in (1) and (2) [38].

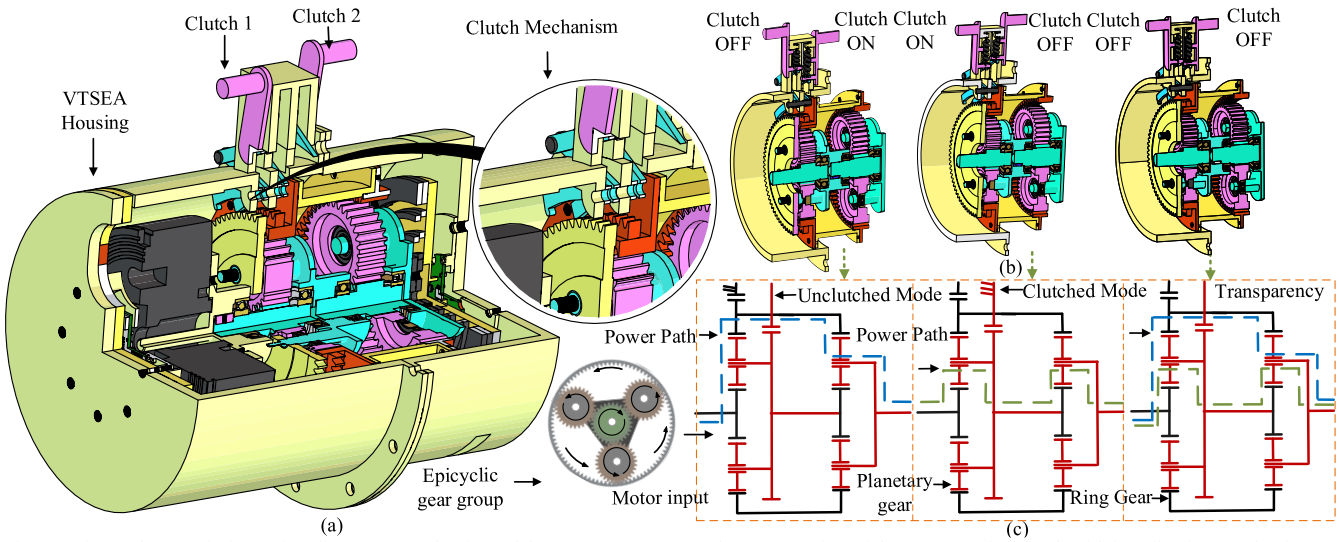

Fig. 2. Drive and transmission ratio adjustment mechanism of the VTSEA. (a) Internal representation of the VTSEA. (b) Clutch with its adjusting mechanism. (c) Power path of the epicyclic gear with the movement of the Clutch.

In which $\boldsymbol{q}(t) \in \mathbb{R}^n$ and $\boldsymbol{\theta}(t) \in \mathbb{R}^n$ are joint and motor angular displacements, respectively, $M(\boldsymbol{q}) \in \mathbb{R}^n$ are inertia matrices of rigid parts, $C(\boldsymbol{q}, \dot{\boldsymbol{q}}) \in \mathbb{R}^n$ are Centripetal-Coriolis and viscous friction matrices of rigid links, $D(\dot{\boldsymbol{q}}) \in \mathbb{R}^n$ are Inertia correction matrix of the motor side, $G(\boldsymbol{q}) \in \mathbb{R}^n$ denotes a gravitational torque, $J \in \mathbb{R}^n$ and $K \in \mathbb{R}^n$ are inertia and stiffness matrices of VTSEA, respectively. $\boldsymbol{\tau}_m \in \mathbb{R}^n$ is a control input. In this brief, assume that $\boldsymbol{q}$, $\dot{\boldsymbol{q}}$, $\boldsymbol{\theta}$, and $\dot{\boldsymbol{\theta}}$ are observable measurements, the specific forms of (1) and (2) are hard to know, and the following properties and definitions are given for system analysis and control law deducing.

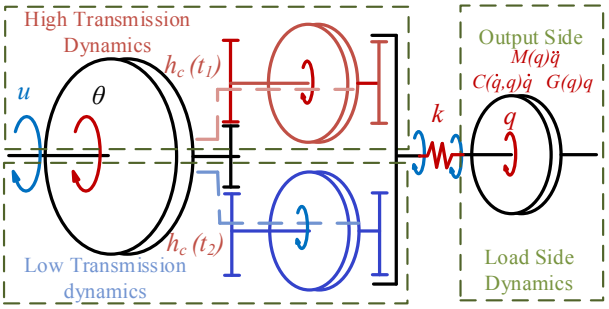

Fig. 3 Two mass models of VTSEA.

$$M(\boldsymbol{q})\ddot{q} + C(\boldsymbol{q}, \dot{\boldsymbol{q}})\dot{\boldsymbol{q}} + G(\boldsymbol{q}) = \boldsymbol{\tau} \tag{1}$$

$$(J - h_c(t)D(\dot{\boldsymbol{\theta}}))\ddot{\boldsymbol{\theta}} + \boldsymbol{\tau} = \boldsymbol{\tau}_m \tag{2}$$

$$\boldsymbol{\tau} = K(\boldsymbol{\theta} - \boldsymbol{q}) \tag{3}$$

where $h_c(t)$ is defined as a switching variable equal to 1 when the VTSEA is in the high transmission ratio and to 0 when it is in the low transmission ratio.

Property 1 [38]: $M(\boldsymbol{q})$, $C(\boldsymbol{q}, \dot{\boldsymbol{q}})$, $D(\dot{\boldsymbol{\theta}})$ and $G(\boldsymbol{q})$ are of C^1, $\forall \boldsymbol{q} \in \mathbb{R}^n$ and $\forall \dot{\boldsymbol{q}} \in \mathbb{R}^n$, and D, $J - h_c(t)D(\dot{\boldsymbol{\theta}})$, and K are diagonal and constant.

Property 2 [38]: $M(\boldsymbol{q})$ is symmetric positive-definite, $\forall \boldsymbol{q} \in \mathbb{R}^n$, and D, J, and K are positive-definite and diagonal.

Property 3 [39, 40]: $\dot{\boldsymbol{M}}(q) - 2\boldsymbol{C}(q, \dot{q})$ is a skew symmetric, $\forall \boldsymbol{q} \in \mathbb{R}^n$.

Property 4 [39, 40]: $x^T \left(\frac{1}{2}\dot{M}(\boldsymbol{q}) - C(\boldsymbol{q}, \dot{\boldsymbol{q}})\right) x = 0$, $\forall \boldsymbol{x} \in \mathbb{R}^n$, and $M(\boldsymbol{q})$ is symmetric positive-definite.

Since the VTSEA system has fast mechanical dynamics (4) and slow mechanical dynamics (5), thus displaying the two-timescale behavior [17]. Hence, the SPT is able to be used to design controllers for two separate subsystems by regarding the fast dynamics (4) as perturbations of the slow dynamics (5).

First, the overall control input of the VTSEA is expressed as

$$\boldsymbol{\tau}_m = \boldsymbol{\tau}_s + \boldsymbol{\tau}_f \tag{3}$$

where τ_s and τ_f are the slow subsystem control input and the fast subsystem control input, respectively.

The fast time scale can be described as

$$(J - h_c(t)D(\dot{\boldsymbol{\theta}}))K^{-1}\ddot{\boldsymbol{\tau}} + \boldsymbol{\tau} = \boldsymbol{\tau_m} - (J - h_c(t)D(\dot{\boldsymbol{\theta}}))\ddot{\boldsymbol{q}} \tag{4}$$

The spring stiffness K can be also expressed as $K = K_1 / \varepsilon^2$, in which $\varepsilon \in \mathbb{R}^+$ is a small constant, and $K_0 \in \mathbb{R}^n$. Then, substituting it into (4) yields

$$\varepsilon^2(J - h_c(t)D(\dot{\boldsymbol{\theta}}))\ddot{\boldsymbol{\tau}} + K_1\boldsymbol{\tau} = K_1(\boldsymbol{\tau_s} + \boldsymbol{\tau_f} - (J - h_c(t)D(\dot{\boldsymbol{\theta}}))\ddot{\boldsymbol{q}}) \tag{5}$$

Define $\boldsymbol{\tau_f} = -K_v\dot{\boldsymbol{\tau}} = -\varepsilon K_2\dot{\boldsymbol{\tau}}$, where K_v is the differential feedback gain of $\boldsymbol{T}$, and K_2 is used to stabilize $\boldsymbol{\tau_f}$. Substitute (5) into (6). Then, the fast subsystem can be expressed as

$$\varepsilon^2\left(J - h_c(t)D(\dot{\boldsymbol{\theta}})\right)K(\ddot{\boldsymbol{\theta}} - \ddot{\boldsymbol{q}}) + \varepsilon K_1K_2(\dot{\boldsymbol{\theta}} - \dot{\boldsymbol{q}}) + K_1K(\boldsymbol{\theta} - \boldsymbol{q}) = K_1(\boldsymbol{\tau_s} - (J - h_c(t)D(\dot{\boldsymbol{\theta}}))\ddot{\boldsymbol{q}}) \tag{6}$$

The system expressed by (6) and (1) can be written in the standard SPT form. With $\varepsilon = 0$, the slow subsystem is given by

$$\left(M(\boldsymbol{q}) + (J - h_c(t)D(\dot{\boldsymbol{\theta}}))\right)\ddot{\boldsymbol{q}} + C(\boldsymbol{q}, \dot{\boldsymbol{q}})\dot{\boldsymbol{q}} + g(\boldsymbol{q}) = \boldsymbol{\tau_s} \tag{7}$$

Define

$$u_e = \boldsymbol{\tau_m} - (J - h_c(t)D(\dot{\boldsymbol{\theta}}))\ddot{\boldsymbol{q}} \quad (8)$$

This is equal to having a filter between u_e and the torque τ due to the VTSEA's flexible K^{-1}. The bandwidth of this filter will increase with increasing K^{-1}. To compensate for the inertial of VTSEA, a new VTSEA control input is defined as

$$\boldsymbol{\tau_m} = K_a\boldsymbol{u_a} + \boldsymbol{u_f} \quad (9)$$

where $\boldsymbol{u_a}$ is the new control input, $\boldsymbol{u_f}$ is the inertial compensation and K_a is a parameter matrix to adjust the low-frequency gain of the filter.

Substituting (14) into (9) yields

$$(J - h_c(t)D(\dot{\boldsymbol{\theta}}))K^{-1}\ddot{\boldsymbol{\tau}} + \boldsymbol{\tau} = k_a\boldsymbol{u_a} + \boldsymbol{u_f} - (J - h_c(t)D(\dot{\boldsymbol{\theta}}))\ddot{\boldsymbol{q}} \quad (10)$$

Then

$$(J - h_c(t)D(\dot{\boldsymbol{\theta}}))K^{-1}\ddot{\boldsymbol{\tau}} + \boldsymbol{\tau} = k_a\left(\boldsymbol{u_a} - \frac{1}{k_a}J\ddot{\boldsymbol{q}}\right) + \boldsymbol{u_f} \quad (11)$$

Let $\boldsymbol{u_1} = \boldsymbol{u_a} - \frac{1}{k_a}(J - h_c(t)D(\dot{\boldsymbol{\theta}}))\ddot{\boldsymbol{q}}$ and $\boldsymbol{u_f} = -K_{tp}\boldsymbol{T}$, where K_{tp} is the flexible compensation coefficient which can be adjusted. Then substitute them into (11) yields

$$(J - h_c(t)D(\dot{\boldsymbol{\theta}}))K^{-1}\ddot{\boldsymbol{\tau}} + \boldsymbol{\tau} = k_a\boldsymbol{u_1} - K_{tp}\boldsymbol{\tau} \quad (12)$$

Then

$$(J - h_c(t)D(\dot{\boldsymbol{\theta}}))K^{-1}\ddot{\boldsymbol{\tau}} + (I + K_{tp})\boldsymbol{\tau} = k_a\boldsymbol{u_1} \quad (13)$$

To ensure the u_f have an appropriate low-frequency gain, choose $K_a = I + K_{tp}$, then substitute it to (13) yields

$$(J - h_c(t)D(\dot{\boldsymbol{\theta}}))K_a^{-1}K^{-1}\ddot{\boldsymbol{\tau}} + \boldsymbol{\tau} = \boldsymbol{u_1} \quad (14)$$

Let $K_e = K \cdot K_a = K(I + K_{tp})$, which is the equivalent stiffness of VTSEA.

Then

$$(J - h_c(t)D(\dot{\boldsymbol{\theta}}))K_e^{-1}\ddot{\boldsymbol{\tau}} + \boldsymbol{\tau} = \boldsymbol{u_a} - K_a^{-1}J\ddot{\boldsymbol{q}} \quad (15)$$

From (15), we can see that K_e is adjustable, and the bandwidth of inner torque can be increased enhancing K_e.

Define a new control input

$$\boldsymbol{u_a} = \boldsymbol{u_{as}} + \boldsymbol{u_{af}} \quad (16)$$

Let

$$\boldsymbol{u_{af}} = -K_{av}\dot{\boldsymbol{\tau}}, K_e = \frac{K_{a1}}{\mu^2}, K_{av} = \mu K_{a2} \quad (17)$$

where μ is a small parameter, K_{a1} is the parameter matrices, K_{av} is the new torque control feedback gain and K_{a2} is used to stabilize $\boldsymbol{\tau_f}$. Then substitute them to (15) yields

$$(J - h_c(t)D(\dot{\boldsymbol{\theta}}))\mu^2K_{a1}^{-1}\ddot{\boldsymbol{\tau}} + \boldsymbol{\tau} = \boldsymbol{u_{as}} - \mu K_{a2}\dot{\boldsymbol{\tau}} - K_a^{-1}(J - h_c(t)D(\dot{\boldsymbol{\theta}}))\ddot{\boldsymbol{q}} \quad (18)$$

Then

$$\mu^2(J - h_c(t)D(\dot{\boldsymbol{\theta}}))\ddot{\boldsymbol{\tau}} + K_{a1}\boldsymbol{\tau} = K_{a1}\boldsymbol{u_{as}} - \mu K_{a1}K_{a2}\dot{\boldsymbol{\tau}} - (J - h_c(t)D(\dot{\boldsymbol{\theta}}))\ddot{\boldsymbol{q}} \quad (19)$$

That is equal to

$$\mu^2J\ddot{\boldsymbol{\tau}} + \mu K_{a1}K_{a2}\dot{\boldsymbol{\tau}} + K_{a1}\boldsymbol{\tau} = K_{a1}(u_{as} - K_a^{-1} - \mu K_{a1}K_{a2}\dot{\boldsymbol{\tau}} - (J - h_c(t)D(\dot{\boldsymbol{\theta}}))\ddot{\boldsymbol{q}}) \quad (20)$$

With $\mu = 0$, and the quasi-steady system equation is:

$$\boldsymbol{\tau} = \boldsymbol{u_{as}} - K_a^{-1}(J - h_c(t)D(\dot{\boldsymbol{\theta}}))\ddot{\boldsymbol{q}} \quad (21)$$

Substitute it to (1) yields

$$M(\boldsymbol{q})\ddot{\boldsymbol{q}} + C(\boldsymbol{q},\dot{\boldsymbol{q}})\dot{\boldsymbol{q}} + g(\boldsymbol{q}) = \boldsymbol{u_{as}} - K_a^{-1}(J - h_c(t)D(\dot{\boldsymbol{\theta}}))\ddot{\boldsymbol{q}} \quad (22)$$

Then

$$\left(M(\boldsymbol{q}) + K_a^{-1} = \boldsymbol{u_{as}} - K_a^{-1}(J - h_c(t)D(\dot{\boldsymbol{\theta}}))\right)\ddot{\boldsymbol{q}} + C(\boldsymbol{q},\dot{\boldsymbol{q}})\dot{\boldsymbol{q}} + g(\boldsymbol{q}) = \boldsymbol{u_{as}} \quad (23)$$

Define $M_e(\boldsymbol{q},\dot{\boldsymbol{\theta}}) = M(\boldsymbol{q}) + K_a^{-1}(J - h_c(t)D(\dot{\boldsymbol{\theta}}))$, then we can get the new slow system is:

$$M_e(\boldsymbol{q},\dot{\boldsymbol{\theta}})\ddot{\boldsymbol{q}} + C(\boldsymbol{q},\dot{\boldsymbol{q}})\dot{\boldsymbol{q}} + g(\boldsymbol{q}) = \boldsymbol{u_{as}} \quad (24)$$

Based on (3), the desired torque $\boldsymbol{\tau_{desired}}$ and the desired position of VTSEA has the form

$$\boldsymbol{\tau_{desired}} = K(\boldsymbol{\theta} - \boldsymbol{q}) \quad (25)$$

Let

$$\boldsymbol{y} = (\dot{\boldsymbol{q}}_{\boldsymbol{d}} - \dot{\boldsymbol{q}}) - \lambda(\boldsymbol{q_d} - \boldsymbol{q}) \quad (26)$$

$$\dot{\boldsymbol{\sigma}} = \dot{\boldsymbol{q}}_{\boldsymbol{d}} - \lambda(\boldsymbol{q_d} - \boldsymbol{q}) \quad (27)$$

$$\boldsymbol{w}^T = [M_e(\boldsymbol{q},\dot{\boldsymbol{\theta}}) \quad C(\boldsymbol{q},\dot{\boldsymbol{q}}) \quad g(\boldsymbol{q})] \quad (28)$$

$$\boldsymbol{x} = [\ddot{\boldsymbol{\sigma}} \quad \dot{\boldsymbol{\sigma}} \quad 1]^T \quad (29)$$

where λ is a positive coefficient, $\boldsymbol{q_d}$ is desired joint angular positions, and $\boldsymbol{q}$ is actual joint angular positions.

Substitute (26) and (27) into (23) yields

$$M_e(\boldsymbol{q},\dot{\boldsymbol{\theta}})\dot{\boldsymbol{y}} + C(\boldsymbol{q},\dot{\boldsymbol{q}})\boldsymbol{y} = \boldsymbol{w}^T\boldsymbol{x} - \boldsymbol{u_{as}} \quad (30)$$

Therefore, the control law for the slow subsystem is

$$\boldsymbol{u_{as}} = \boldsymbol{w}^T\tilde{\boldsymbol{x}} + K_d\boldsymbol{y} \quad (31)$$

where K_d is positive-define and diagonal, $\tilde{\boldsymbol{x}}$ is the estimated value of $\boldsymbol{x}$. $\tilde{\boldsymbol{x}}$ can be obtained from the following equations [41]:

$$\dot{\tilde{\boldsymbol{x}}} = Proj(\boldsymbol{wy}, \tilde{x}), \|\tilde{x}(0)\| \le \boldsymbol{\delta} \quad (32)$$

where $\boldsymbol{\delta}$ is the maximum nominal value of the VTSEA dynamic parameters.

Then, from (9) the torque controller input of the VTSEA is

$$\boldsymbol{\tau_m} = (1 + K_{tp})\boldsymbol{u_a} - K_{tp}\boldsymbol{\tau} = (1 + K_{tp})(\boldsymbol{w}^T\tilde{\boldsymbol{x}} + K_d\boldsymbol{y} - K_{av}\dot{\boldsymbol{\tau}}) - K_{tp}K(\boldsymbol{\theta} - \boldsymbol{q}) = (1 + K_{tp})([M_e(\boldsymbol{q},\dot{\boldsymbol{\theta}}) \quad C(\boldsymbol{q},\dot{\boldsymbol{q}}) \quad g(\boldsymbol{q})] \cdot \tilde{\boldsymbol{x}} + K_d\boldsymbol{y} - K_{av}K(\dot{\boldsymbol{\theta}} - \dot{\boldsymbol{q}})) - K_{tp}K(\boldsymbol{\theta} - \boldsymbol{q}) \quad (33)$$

D. Proof of the System Stability

Before experiments, the stability of the system should be

proved. The stability of the fast subsystem (20) can be guaranteed by choosing an appropriate K_{a2} in the control low (17).

For the slow subsystem (24) and control law (31), consider the following Lyapunov function:

$$V_1 = \frac{1}{2}\left(\boldsymbol{y}^T M_e(\boldsymbol{q},\dot{\boldsymbol{\theta}})\boldsymbol{y} + (\boldsymbol{x}-\tilde{\boldsymbol{x}})^T(\boldsymbol{x}-\tilde{\boldsymbol{x}})\right) \tag{34}$$

The first derivative of the Lyapunov function of the control system is defined as follows:

$$\dot{V}_1 = \boldsymbol{y_T} M_e(\boldsymbol{q},\dot{\boldsymbol{\theta}})\dot{\boldsymbol{y}} + \frac{1}{2}\boldsymbol{y_T}\dot{M}_e(\boldsymbol{q},\dot{\boldsymbol{\theta}}) + \left(\dot{\boldsymbol{x}}-\dot{\tilde{\boldsymbol{x}}}\right)^T(\boldsymbol{x}-\tilde{\boldsymbol{x}}) \tag{35}$$

Since

$$M_e(\boldsymbol{q},\dot{\boldsymbol{\theta}})\dot{\boldsymbol{y}} = -C(\boldsymbol{q},\dot{\boldsymbol{q}})y + \boldsymbol{w}^T(\boldsymbol{x}-\tilde{\boldsymbol{x}}) - K_d\boldsymbol{y} \tag{36}$$

Substitute (35) to (34) yields

$$\begin{aligned}\dot{V}_1 &= \boldsymbol{y}^T(-C(\boldsymbol{q},\dot{\boldsymbol{q}})\boldsymbol{y} + \boldsymbol{w}^T(\boldsymbol{x}-\tilde{\boldsymbol{x}}) - K_d\boldsymbol{y}) \\ &+ \frac{1}{2}\boldsymbol{y_T}\dot{M}_e(\boldsymbol{q},\dot{\boldsymbol{\theta}})\boldsymbol{y} + \left(\dot{\boldsymbol{x}}-\dot{\tilde{\boldsymbol{x}}}\right)^T(\boldsymbol{x}-\tilde{\boldsymbol{x}}) \\ &= \frac{1}{2}\boldsymbol{y}^T\left(\dot{M}_e(\boldsymbol{q},\dot{\boldsymbol{\theta}}) - 2C(\boldsymbol{q},\dot{\boldsymbol{q}})\right)\boldsymbol{y} - \boldsymbol{y}^T K_d\boldsymbol{y} \\ &+ \left(\boldsymbol{y}^T\boldsymbol{w}^T + \left(\dot{\boldsymbol{x}}-\dot{\tilde{\boldsymbol{x}}}\right)^T\right)(\boldsymbol{x}-\tilde{\boldsymbol{x}})\end{aligned} \tag{37}$$

From *Property 4,* we can get

$$\dot{M}_e(\boldsymbol{q},\dot{\boldsymbol{\theta}}) - 2C(\boldsymbol{q},\dot{\boldsymbol{q}}) = 0 \tag{38}$$

Since x is a constant vector, then

$$\left(\dot{\boldsymbol{x}}-\dot{\tilde{\boldsymbol{x}}}\right)^T = -\dot{\tilde{\boldsymbol{x}}}^T = -(Proj(\boldsymbol{wy},\tilde{\boldsymbol{x}}))^T \tag{39}$$

Substitute (37) and (38) into (36) yields

$$\begin{aligned}\dot{V}_1 &= -\boldsymbol{y}^T K_d\boldsymbol{y} \\ &+ (\boldsymbol{wy})^T(\boldsymbol{x}-\tilde{\boldsymbol{x}}) - (Proj(\boldsymbol{wy},\tilde{\boldsymbol{x}}))^T(\boldsymbol{x}-\tilde{\boldsymbol{x}})\end{aligned} \tag{40}$$

Since

$$(\boldsymbol{x}-\tilde{\boldsymbol{x}})^T Proj(\boldsymbol{wy},\tilde{\boldsymbol{x}}) \geq (\boldsymbol{x}-\tilde{\boldsymbol{x}})^T\boldsymbol{wy} \tag{41}$$

Therefore

$$\dot{V}_1 \leq -\boldsymbol{y}^T K_d\boldsymbol{y} < 0 \tag{42}$$

As a result, the slow subsystem is asymptotically stable.

Then, consider the following Lyapunov function of the entire system:

$$V = \alpha V_1 + \beta V_2 \tag{43}$$

where V_1 and V_2 are the Lyapunov function of the slow subsystem and fast subsystem, respectively, and α, β are positive constants. And we can know that V is positive definite, and $\dot{V} = \alpha\dot{V}_1 + \beta\dot{V}_2$ is negative definite based on the former analysis. Thus, we can conclude that the entire system is asymptotically stable.

III. Experiments and Results

After the stability of the control system is verified, the following experiments should be conducted to prove the feasibility of the entire system. The electronic hardware system is shown in Fig. 4. The controller is implemented in the Dspace 1202. It's worth mentioning that the following experiments are just preliminary arrangements to validate the characteristics of the VTSEA.

1) To test the output stiffness of the VTSEA.
2) To Test the back drivability of the VTSEA.
3) To test the SP-based torque controller's performance.

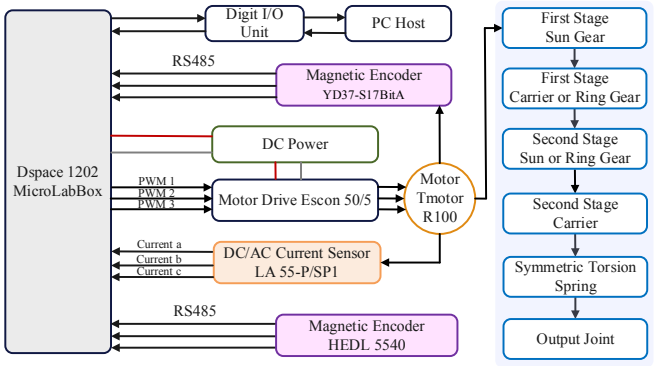

Fig. 4. Electronic hardware system of VTSEA.

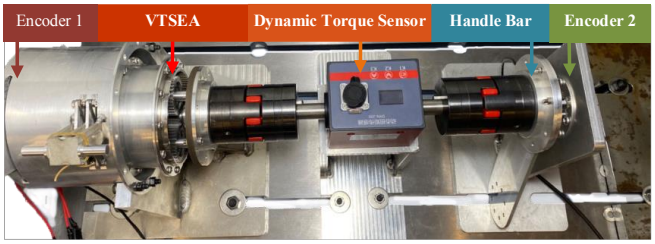

(a)

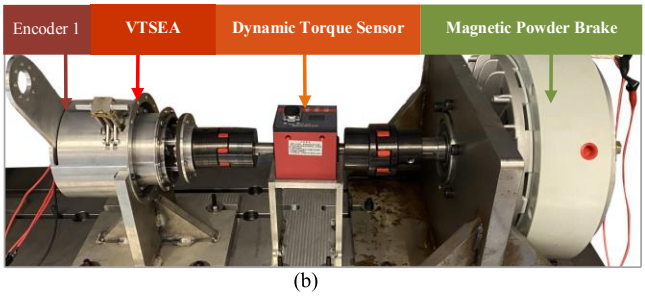

(b)

Fig. 5. VTSEA test bench. (a) Stiffness measuring and back drivability test bench. (b) SP-based torque controller test bench, one of the dynamic torque sensors (DYN-200) is linked to the output end of the VTSEA, the other end of which is combined with the magnetic power brake or the handlebar.

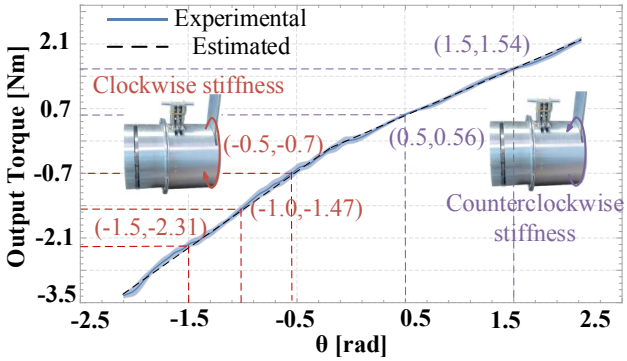

Fig. 6. Stiffness of the VTSEA. (a) Stiffness relationship under the high transmission ratio. (b) Stiffness relationship under the low transmission ratio.

Experiment I: To test the output angle stiffness of the VTSEA, the experimental system structure is described in Fig. 4, and the test bench is shown in Fig. 5 (a). The deflection angle in 20 increments between the maximum flexion and

extension angles is applied on the handlebar, and the measuring data from the dynamic torque sensor and two encoders is recorded simultaneously. This is a repeated test at intervals of 20° from -150° to 150°, and five tests for each angle. The output stiffness of clockwise and counterclockwise of the VTSEA is calculated from Fig. 6.

Experiment II: To test the back-drivability of the VTSEA, with the housing of VTSEA locked on the experimental bench and the controller closed the output end of the VTSEA was manually shaken within -60° to 60° at frequencies of 0.2 to 0.5 Hz. The measured data from both encoders are recorded and employed to estimate the interaction torque. The measured output angle and back drive torque are described in Fig. 7. The results show that the back drive torque of the VTSEA is 0.3 N.m and 0.75 N.m, at a low transmission ratio and high transmission ratio, respectively.

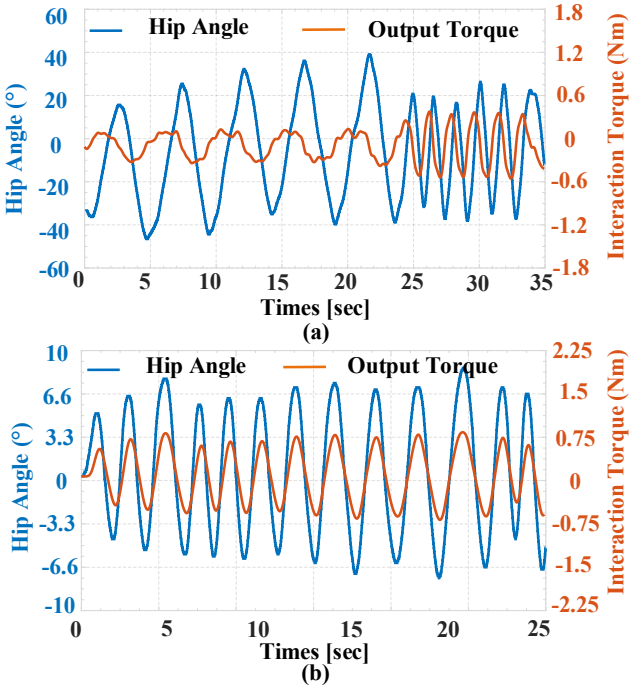

Fig. 7. Back drivability test of the VTSEA in the unpowered condition. (a) Back drivability test results in the low transmission ratio mode. (b) Back drivability test result in the high transmission ratio mode.

Experiment III: To assess the performance of the SPT-based torque controller, torque tracking experiments of sinusoidal input with an angular frequency of $\pi/2$ rad/s are conducted. The experimental platform for VTSEA is presented in Fig. 5 (b). The magnetic powder brake can fix the output end of the VTSEA at different angles. Fig. 8 (a) is the torque-tacking example of SPT-based torque control with a reference of $\tau_d = 1.0\sin(\frac{\pi}{2}t)$, and Fig. 8 (b) shows the tracking error result, the final error reaches an approximate value of 0.07 N.m. The torque input tracking results demonstrate the proposed SPT-based torque controller can precisely output the desired torque. The root mean square (RMS) error between the desired torque and the actual output torque measured by the torsional springs and two encoders is approximately 0.0314 N.m.

IV. Conclusion and Future Work

In this article, we presented and tested a VTSEA for hip exoskeletons. The VTSEA actuation consists of a motor and the transmission adjustment mechanism. It can generate a high torque of 133.2 N.m nominal torque with a weight of 5.98 kg. The proposed VTSEA achieves a high torque density of 22.3 N.m/kg. Based on this developed VTSEA, a lightweight bilateral portable hip exoskeleton is designed, which performs high back drivability of 0.3 N.m and stable torque tracking performance, demonstrating its outstanding torque delivery ability. With the proposed SPT-based torque controller, VTSEA produced a small torque tracking error of 0.0314 N.m.

In the near future, we will conduct more characterizing experiments and design a high-level controller that includes an estimation of the user's intention. Also, we will assign a natural assistance torque profile corresponding to each gait phase. Complementary subject experiments will be conducted to validate the entire exoskeleton's performance under transparency mode, low transmission ratio assisting mode, and high transmission ratio assisting mode. Further design optimization should be conducted to minimize the size of the exoskeleton to make our device useful for clinical application.

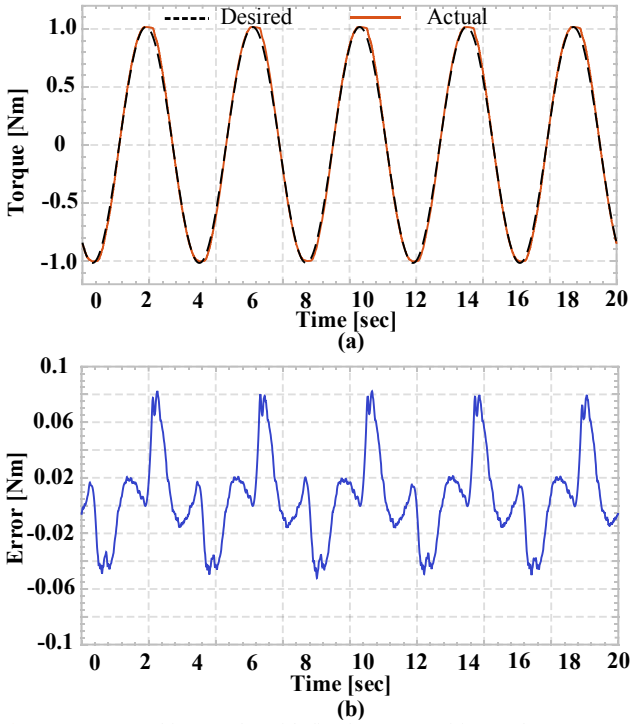

Fig. 8. Torque tracking results with fixed output position to demonstrate the performance of torque tracking. (a) Sinusoidal response of 1 N.m periodic input. (b) Tracking error of the torque controller.

References

[1] T. Zhang and J. Xia, "Interconnection and damping assignment passivity-based impedance control of a compliant assistive robot for physical human–robot interactions," *IEEE Robotics and Automation Letters,* vol. 4, no. 2, pp. 538-545, 2019.

[2] Y. Pan, X. Li, and H. Yu, "Efficient PID tracking control of robotic manipulators driven by compliant actuators," *IEEE Transactions on Control Systems Technology,* vol. 27, no. 2, pp. 915-922, 2018.

[3] G. Aguirre-Ollinger and H. Yu, "Lower-limb exoskeleton with variable-structure series elastic actuators: Phase-synchronized force

control for gait asymmetry correction," *IEEE Transactions on Robotics,* vol. 37, no. 3, pp. 763-779, 2020.
[4] T. Zhang, C. Ning, Y. Li, and M. Wang, "Design and Validation of a Lightweight Hip Exoskeleton Driven by Series Elastic Actuator With Two-Motor Variable Speed Transmission," *IEEE Transactions on Neural Systems and Rehabilitation Engineering,* vol. 30, pp. 2456-2466, 2022.
[5] D. E. Lieberman, A. G. Warrener, J. Wang, and E. R. Castillo, "Effects of stride frequency and foot position at landing on braking force, hip torque, impact peak force and the metabolic cost of running in humans," *Journal of Experimental Biology,* vol. 218, no. 21, pp. 3406-3414, 2015.
[6] C. Camardella, F. Porcini, A. Filippeschi, S. Marcheschi, M. Solazzi, and A. Frisoli, "Gait phases blended control for enhancing transparency on lower-limb exoskeletons," *IEEE Robotics and Automation Letters,* vol. 6, no. 3, pp. 5453-5460, 2021.
[7] Y. Qian, S. Han, Y. Wang, H. Yu, and C. Fu, "Toward improving actuation transparency and safety of a hip exoskeleton with a novel nonlinear series elastic actuator," *IEEE/ASME Transactions on Mechatronics,* vol. 28, no. 1, pp. 417-428, 2022.
[8] W. Huo *et al.*, "Impedance modulation control of a lower-limb exoskeleton to assist sit-to-stand movements," *IEEE Transactions on Robotics,* vol. 38, no. 2, pp. 1230-1249, 2021.
[9] W. Huo, S. Mohammed, and Y. Amirat, "Impedance reduction control of a knee joint human-exoskeleton system," *IEEE Transactions on Control Systems Technology,* vol. 27, no. 6, pp. 2541-2556, 2018.
[10] S. Kim and J. Bae, "Force-mode control of rotary series elastic actuators in a lower extremity exoskeleton using model-inverse time delay control," *IEEE/ASME Transactions on Mechatronics,* vol. 22, no. 3, pp. 1392-1400, 2017.
[11] D. Zanotto, T. Lenzi, P. Stegall, and S. K. Agrawal, "Improving transparency of powered exoskeletons using force/torque sensors on the supporting cuffs," in *2013 IEEE 13th international conference on rehabilitation robotics (ICORR)*, 2013: IEEE, pp. 1-6.
[12] I. Kang, H. Hsu, and A. Young, "The effect of hip assistance levels on human energetic cost using robotic hip exoskeletons," *IEEE Robotics and Automation Letters,* vol. 4, no. 2, pp. 430-437, 2019.
[13] M. R. Tucker, C. Shirota, O. Lambercy, J. S. Sulzer, and R. Gassert, "Design and characterization of an exoskeleton for perturbing the knee during gait," *IEEE Transactions on Biomedical Engineering,* vol. 64, no. 10, pp. 2331-2343, 2017.
[14] E. Sariyildiz, G. Chen, and H. Yu, "A unified robust motion controller design for series elastic actuators," *IEEE/ASME Transactions on Mechatronics,* vol. 22, no. 5, pp. 2229-2240, 2017.
[15] N. Sun, L. Cheng, X. Xia, and L. Han, "Design and Optimization of an Index Finger Exoskeleton with Semi-Wrapped Fixtures and Series Elastic Actuators," *IEEE Transactions on Neural Systems and Rehabilitation Engineering,* 2023.
[16] C. B. Sanz-Morère *et al.*, "An active knee orthosis with a variable transmission ratio through a motorized dual clutch," *Mechatronics,* vol. 94, p. 103018, 2023.
[17] T. Zhang and H. Huang, "Design and control of a series elastic actuator with clutch for hip exoskeleton for precise assistive magnitude and timing control and improved mechanical safety," *IEEE/ASME Transactions on Mechatronics,* vol. 24, no. 5, pp. 2215-2226, 2019.
[18] S. J. Lee, D. Jin, S. H. Kang, D. Gaebler-Spira, and L.-Q. Zhang, "Combined ankle/knee stretching and pivoting stepping training for children with cerebral palsy," *IEEE Transactions on Neural Systems and Rehabilitation Engineering,* vol. 27, no. 9, pp. 1743-1752, 2019.
[19] F. M. Escalante, L. F. dos Santos, Y. Moreno, A. A. Siqueira, M. H. Terra, and T. Boaventura, "Markovian transparency control of an exoskeleton robot," *IEEE Robotics and Automation Letters,* vol. 8, no. 2, pp. 544-551, 2022.
[20] Y. Qian, H. Yu, and C. Fu, "Adaptive oscillator-based assistive torque control for gait asymmetry correction with a nSEA-driven hip exoskeleton," *IEEE Transactions on Neural Systems and Rehabilitation Engineering,* vol. 30, pp. 2906-2915, 2022.
[21] J. Song, A. Zhu, Y. Tu, X. Zhang, and G. Cao, "Novel design and control of a crank-slider series elastic actuated knee exoskeleton for compliant human–robot interaction," *IEEE/ASME Transactions on Mechatronics,* vol. 28, no. 1, pp. 531-542, 2022.
[22] Y. Qian, S. Han, G. Aguirre-Ollinger, C. Fu, and H. Yu, "Design, modeling, and control of a reconfigurable rotary series elastic actuator with nonlinear stiffness for assistive robots," *Mechatronics,* vol. 86, p. 102872, 2022.
[23] S. Oh and K. Kong, "High-precision robust force control of a series elastic actuator," *IEEE/ASME Transactions on mechatronics,* vol. 22, no. 1, pp. 71-80, 2016.
[24] D. Cheon, K. Nam, and S. Oh, "Design and Robust Control of a Precise Torque Controllable Steering Module for Steer-by-Wire Systems," *IEEE Transactions on Industrial Electronics,* vol. 69, no. 12, pp. 13245-13254, 2022.
[25] D. Kim, K. Koh, G.-R. Cho, and L.-Q. Zhang, "A robust impedance controller design for series elastic actuators using the singular perturbation theory," *IEEE/ASME Transactions on Mechatronics,* vol. 25, no. 1, pp. 164-174, 2019.
[26] H. K. Khalil, *Nonlinear Systems*. Prentice Hall, 2002.
[27] M. W. Spong, "Adaptive control of flexible joint manipulators: Comments on two papers," *Automatica,* vol. 31, no. 4, pp. 585-590, 1995.
[28] J. Yuan and Y. Stepanenko, "Composite adaptive control of flexible joint robots," *Automatica,* vol. 29, no. 3, pp. 609-619, 1993.
[29] C. Wang *et al.*, "A Lightweight Series Elastic Actuator With Variable Stiffness: Design, Modeling, and Evaluation," *IEEE/ASME Transactions on Mechatronics,* 2023.
[30] I. Kang, R. R. Peterson, K. R. Herrin, A. Mazumdar, and A. J. Young, "Design and validation of a torque-controllable series elastic actuator-based hip exoskeleton for dynamic locomotion," *Journal of Mechanisms and Robotics,* vol. 15, no. 2, p. 021007, 2023.
[31] O. S. Al-Dahiree, R. A. R. Ghazilla, M. O. Tokhi, H. J. Yap, and E. A. Albaadani, "Design of a compact energy storage with rotary series elastic actuator for lumbar support exoskeleton," *Machines,* vol. 10, no. 7, p. 584, 2022.
[32] P. V. Kokotović, "Applications of singular perturbation techniques to control problems," *SIAM review,* vol. 26, no. 4, pp. 501-550, 1984.
[33] Y. Luo and C. Liu, "A flux constrained predictive control for a six-phase PMSM motor with lower complexity," *IEEE Transactions on Industrial Electronics,* vol. 66, no. 7, pp. 5081-5093, 2018.
[34] J. Yu, C. Liu, Z. Song, and H. Zhao, "Permeance and inductance modeling of a double-stator hybrid-excited flux-switching permanent-magnet machine," *IEEE Transactions on Transportation Electrification,* vol. 6, no. 3, pp. 1134-1145, 2020.
[35] R. Huang, Z. Song, H. Zhao, and C. Liu, "Overview of axial-flux machines and modeling methods," *IEEE Transactions on Transportation Electrification,* vol. 8, no. 2, pp. 2118-2132, 2022.
[36] H. Zhao, C. Liu, Z. Song, and S. Liu, "Design and control of a new compound double-rotor electric machine for hybrid propulsion system," *IEEE Transactions on Power Electronics,* vol. 37, no. 3, pp. 3283-3296, 2021.
[37] R. Huang, Z. Dong, B. Zhang, and C. Liu, "Decoupled Modulation Strategy for Harmonic Current Suppression in Five-Phase Series-End Winding PMSM Drives," *IEEE Transactions on Industrial Electronics,* 2024.
[38] D. J. Braun *et al.*, "Robots driven by compliant actuators: Optimal control under actuation constraints," *IEEE Transactions on Robotics,* vol. 29, no. 5, pp. 1085-1101, 2013.
[39] R. Ortega and M. W. Spong, "Adaptive motion control of rigid robots: A tutorial," *Automatica,* vol. 25, no. 6, pp. 877-888, 1989.
[40] J.-J. E. Slotine and W. Li, "On the adaptive control of robot manipulators," *The international journal of robotics research,* vol. 6, no. 3, pp. 49-59, 1987.
[41] J.-B. Pomet and L. Praly, "Adaptive nonlinear regulation: Estimation from the Lyapunov equation," *IEEE Transactions on automatic control,* vol. 37, no. 6, pp. 729-740, 1992.